NJC

ROYAL SOCIETY OF CHEMISTRY

PAPER

View Article Online
View Journal | View Issue

Cite this: *New J. Chem.*, 2024, **48**, 18219

Europium and cobalt modified MOF-808: a humidity-responsive fluorescent barcode†

Nele Marquardt and Andreas Schaate *

Stimuli-responsive luminescent materials can be used to design anti-counterfeit barcodes because even small changes in environmental conditions, such as temperature or the molecules present, can lead to changes in the fluorescence behavior of the materials, enabling dynamic information encoding. Metal–organic frameworks (MOFs) are promising materials for the design of stimuli-responsive barcodes, as their modular structure allows fine tuning of the fluorescence, which in turn can be switched in response to external stimuli. In this work, we present a humidity-responsive fluorescent barcode prototype based on europium- and cobalt-modified MOF-808, which exhibits fluorescence switching in response to changes in relative humidity. The combination of cobalt and europium cations in the same material, along with the coordination ligands on the cobalt cations, are crucial for the functionality of this barcode. By selectively suppressing the fluorescence of europium through the absorption of cobalt complexes in the same energy range, the initial fluorescence intensity of the material can be adjusted. The additional coordination of water molecules to the cobalt centers leads to the formation of cobalt complexes with higher ligand field splitting energy, resulting in a stepwise reactivation of the emission of the europium cations. This can be readily accomplished by exposing the material to different relative humidities. As a result, the barcode provides a higher level of security, as its decoding must be performed under controlled atmospheric conditions, and it is user-friendly since no harmful chemicals are required during the reading process. Additionally, the initial state must be restored before each decoding by heating, as the fluorescence changes dynamically according to the environmental conditions. These characteristics of the material underline the anti-counterfeiting capabilities of the barcode.

Received 5th August 2024,
Accepted 9th October 2024

DOI: 10.1039/d4nj03487b

rsc.li/njc

Introduction

In the modern world, anti-counterfeiting technologies are crucial for ensuring information security and verifying the authenticity of documents like passports, health data and certificates. In addition to commonly used techniques like watermarks, holograms and color changing inks, luminescent materials are increasingly being considered. These materials allow a visible read-out and exhibit a large variability of the output, depending on the manipulation of luminescence during the reading process.[1]

Lanthanide-containing metal–organic frameworks (MOFs) have garnered increasing interests in recent years due to their outstanding fluorescence properties.[2] Lanthanide cations exhibit distinct, characteristic emissions, which have to be sensitized by so-called antenna molecules, like the linker molecules of the MOF, to achieve higher fluorescence intensities.[3] These cations can be incorporated into the inorganic building units (IBUs) of the framework[4] or installed at coordination sites at the linker molecules.[5] In both cases, different types of lanthanide cations can be integrated into the same framework, combining their unique fluorescence properties within a single material.[6]

To enhance information security, the fluorescence of different lanthanides cations has often been combined to generate barcodes, providing additional security through excitation at different wavelengths or varying fluorescence lifetimes.[7] However, superior security can be achieved by developing stimuli-responsive luminescent materials. These materials are designed to exhibit specific fluorescence responses to external stimuli, like changes in temperature,[8] pH,[9] or the presence of solvents, molecules or ions[10] in the environment.

Temperature-dependent changes in the fluorescence are often applied to Ln-MOFs including those containing red-emissive Eu^{3+} and green-emissive Tb^{3+} cations. These changes are induced by varying the efficiency of energy transfer from Tb^{3+} to Eu^{3+}, resulting in a fluorescence color shift. Gao *et al.*[11] presented a heterogeneous bimetallic Ln-MOF constructed by epitaxial growth. They designed barcodes by controlling the doping content of Tb-btc (benzene-1,3,5-tricarboxylate) with europium cations, synthesizing microrods consisting of a central block and two ends. These

Callinstr. 9, 30167, Hannover, Germany. E-mail: andreas.schaate@acb.uni-hannover.de; Fax: +49 511 762 3660; Tel: +49 511 762 3698

† Electronic supplementary information (ESI) available. See DOI: https://doi.org/10.1039/d4nj03487b

barcodes exhibit thermally controlled emission colors and sharp lanthanide emission bands. Heating enhances energy transfer from Tb^{3+} to Eu^{3+}, shifting the fluorescence color from green to yellow in the central block and from yellow to red at the ends, depending on the europium content.

Solvents can also influence the luminescence of lanthanides. For instance, Xia *et al.*[12] demonstrated a europium-based MOF, Eu(bdc)-NH_2 (benzene-1,4-dicarboxylate), which shows water-responsive multicolor fluorescence. Unlike the red emission of europium, the blue linker emission is not affected by an increasing water content in THF, resulting in a luminescent color change from red to blue.

Additionally, molecules and ions can act as luminescence quenchers. Othong *et al.*[13] reported that styrene effectively quenches the luminescence of bimetallic lanthanide-MOFs Eu/Tb-phda (1,4-phenylenediacidic acid). This property was utilized to design a barcode material with MOF ink that is visible under UV light and can be selectively quenched by applying styrene ink. The quenching is self-erasable due to evaporation of styrene within one hour. Similarly, Zhang *et al.*[14] used Ln-MOF ink based on europium or terbium to create patterned boxes. The initial fluorescence was altered by adding various dissolved cations and molecules. For instance, dropping copper(II) solution into specific MOF ink boxes changed the fluorescence from blue to red or violet to green. Further decoding was realized by adding the anti-cancer drugs molecules 6-mercaptopurine (6-MP) and 6-thioguanine (6-TG), resulting in additional fluorescence color changes. This created a three-dimensional (3D) multi-level anti-counterfeiting fluorescent label.

We have designed a barcode responsive to external stimuli. The read-out involves a sequence of exposure to gaseous NH_3, heating to 120 °C and treatment with gaseous HCl, which induces specific fluorescence switching and simultaneous color changes. The materials for the barcode are zirconium-based MOF-808 modified with cobalt or iron cations, respectively, and europium cations. It is embedded in polyvinylidene fluoride to obtain mixed-matrix membranes enabling the arrangement of cut squares in a custom pattern.[15] However, this read-out sequence is not user-friendly, requiring the use of hazardous chemicals.

Initially, both materials exhibit quenched fluorescence, but only Eu,Co-MOF-808 shows an increase in fluorescence at higher relative humidities. This is an unexpected response to water exposure, as O–H vibrations typically quench the fluorescence of lanthanides.[16] Due to these changes in luminescence intensity upon dehydration and rehydration, luminescent Ln-MOFs are being intensively researched for humidity detection.[17–19] For instance, an upconversion luminescent Y/Yb/Er-MOF was demonstrated as a humidity sensor, exhibiting a linear fluorescence quenching response to relative humidity in the range of 11% to 95%, with cyclic stability due to energy absorption by water molecules.[20] However, some humidity sensors have also been reported to exhibit increasing luminescence intensities at elevated humidities. This phenomenon is often attributed to the removal of water molecules, which leads to increased thermal vibrations of the framework, resulting in less effective energy transfer between the ligands and the lanthanide cations. The re-entry of water molecules into the framework results in the formation of hydrogen bonds with the framework, which in turn restores the luminescence intensity.[17] Wang *et al.*[21] reported a luminescent Eu-MOF with 1D pore channels filled with water molecules showing a linear increase in luminescence intensity from 33% to 85%.

Other reported methods for water detection *via* luminescence changes of Ln-MOFs involve the introduction of color-changing functional groups, encapsulation of guests and the insertion of multiple emission centers into the framework.[18,22] Zeng *et al.*[23] demonstrated that colorimetric detection of moisture using a cobalt-containing MOF is also a promising approach. This method is based on a color change from claret red to pink, caused by changes in ligand field energies of the d-orbital of cobalt(II) to the common pink color of a regular octahedral cobalt(II).

Beyond that, the presence of cobalt cations also can affect the fluorescence of europium cations, because of the resonance between the Eu(III) excited states and the broad absorption of Co(II) cations due to d–d transitions. This overlap in absorption bands of transition metal cations and the narrow line emission spectra of lanthanide cations results in the quenching of the Ln(III) emission, with the quenching efficiency depending on the concentration of transition metal cations.[24]

Inspired by these humidity sensor researches, we aim to develop a new read-out method for the Eu,Co-MOF-808 barcode prototype that is user-friendly and realized by varying the relative humidity instead of using hazardous chemicals. Our goal is to clarify how the interplay between cobalt cations in the material and humidity influences fluorescence, enabling targeted fluorescence switching.

Experimental

Materials

Zirconium(IV) chloride (> 99.5%, $ZrCl_4$, Sigma Aldrich), benzene-1,3,5-tricarboxylic acid (95%, trimesic acid, H_3btc, $C_9H_6O_6$, Sigma Aldrich), *N*,*N*-dimethylformamide (≥99.8%, ACS reagent, DMF, C_3H_7NO, Sigma Aldrich), acetic acid (≥99.7%, ASC reagent, CH_3COOH, Sigma Aldrich), hydrochloric acid (37%, ACS reagent, HCl, Sigma Aldrich), acetone (technical, C_3H_6O, Fisher Chemical), ammonium carbonate (EMSURE, ACS reagent, $(NH_4)_2CO_3$, Sigma Aldrich), deuterium oxide (deuteration degree min. 99.95% for NMR spectroscopy, D_2O, Sigma Aldrich), cobalt(II)-chloride hexahydrate (reagent grade, $CoCl_2{\cdot}6H_2O$, Sigma Aldrich), cobalt(II)-acetate tetrahydrate (reagent grade, $Co(C_2H_3O_2)_2{\cdot}4H_2O$, Sigma Aldrich), cobalt(II)-nitrate hexahydrate (reagent grade, $Co(NO_3)_2{\cdot}6H_2O$, Sigma Aldrich), europium(III)-nitrate hexahydrate (99.9%, $Eu(NO_3)_3{\cdot}6H_2O$, Thermo Scientific), methanol (≥99%, MeOH, Roth), poly(vinylidene fluoride) (average $M_w \sim 180\,000$ by GPC, average $M_n \sim 71\,000$, beads or pellets, PVDF, Sigma Aldrich).

Synthesis of MOF-808-FA and -AA

The water-based synthesis of MOF-808-FA and -AA was performed in round-bottom flasks under reflux conditions and stirring, using a modified approach from Farha *et al.*[25]

$ZrCl_4$ (30 mmol, 1 eq.) and H_3btc (10 mmol, 0.33 eq.) were dissolved in a mixture of concentrated HCl (1 mL, 0.4 eq.), formic acid (35 mL, 30.9 eq.) or acetic acid (50 mL, 26.9 eq.), and distilled water (100 mL, 184.7 eq.). The mixture was heated in an oil bath at 110 °C for 24 hours. The resulting white MOF-808-X powder was isolated by centrifugation (6000 rpm, 10 minutes) and washed three times with distilled water and two times with acetone. The powder was pre-dried at 60 °C for at least 2 hours, followed by further drying at 120 °C.

Synthesis of MOF-808

To obtain MOF-808 with a reduced amount of modulators, 4 g MOF-808-FA were extracted with methanol for 27 hours. Afterwards, the white powder was pre-dried at 60 °C for 2 hours, followed by further drying at 120 °C.

Post-synthetic modification with cobalt cations

The incorporation of cobalt cations was performed in DMF. $CoCl_2{\cdot}6H_2O$ (0.5 to 6 eq.) was dissolved in DMF (6.67 mL) by ultrasonication. MOF-808 or MOF-808-AA (100 mg, 1 eq.), respectively, was soaked in the blue solution at rt for one hour, respectively. The powders were isolated by centrifugation (6000 rpm, 10 minutes), washed with DMF until the supernatant became colorless and then washed once with acetone. The blue products were dried at 60 °C.

The post-synthetic modification was also performed using $Co(OAc)_2{\cdot}4H_2O$ (6 eq.) and $Co(NO_3)_2{\cdot}6H_2O$ (6 eq.) as cobalt salts for MOF-808 as described above for one hour. The obtained powders were violet and light blue in color.

Post-synthetic modification of Co-MOF-808 and Co-MOF-808-AA with europium cations

The insertion of europium was performed in acetone at room temperature. $Eu(NO_3)_3{\cdot}6H_2O$ (6 eq.) was dissolved in acetone (3.334 mL) by ultrasonication. Then, Co-MOF-808 or Co-MOF-808-AA (50 mg, 1 eq.), respectively, was soaked in the colorless solution for one hour. After centrifugation (6000 rpm, 10 minutes), the powders were continuously washed until reaching a colorless supernatant. The powders were dried at 60 °C.

Preparation of mixed-matrix membranes

For the preparation of the mixed-matrix membranes (MMMs), the previously reported protocol[15] was slightly modified. Co-MOF-808-AA powder (240 mg), which was synthesized with 0.5 eq., 1 eq. and 5 eq. $CoCl_2{\cdot}6H_2O$, respectively, was dispersed in acetone (10 mL) by ultrasonication for 30 minutes. Simultaneously, polyvinylidene fluoride (160 mg) was dissolved in DMF (2.08 mL) under continuous stirring and gentle heating for 30 minutes. The solution was added to the MOF mixture and mixed again by ultrasonication for 30 minutes. The solvent was then evaporated under reduced pressure. The resulting ink was manually applied to a glass with a doctor blade and heated to 70 °C in an oven without circulating air for at least one hour. The final MMM delaminated from the glass after cooling or was removed with a razor blade.

To generate Eu,Co-MOF-808-AA@PVDF, the cobalt-containing MMMs were cut into strips. The strips were soaked in a solution of $Eu(NO_3)_3{\cdot}6H_2O$ (28 mg) dissolved in acetone (2 mL) for 10 minutes. Afterwards, the strips were washed several times with acetone and dried at 60 °C.

Characterization methods

^{1}H-NMR spectroscopy was conducted at room temperature at 400 MHz using a Bruker BioSpin spectrometer. The samples were dissolved in 0.6 mL of 1 M $(NH_4)_2CO_3$ solution in D_2O under stirring overnight. The spectra were analyzed using TopSpin 4.0.9 software.

Emission spectra were detected using the portable fluorescence spectrometer Indigo from GoyaLab. The samples were placed in a self-designed, 3D-printed measuring cell with two gas ports to enable measurements under gas flow. The samples were covered with a 3D-printed mask and the Indigo spectrometer was placed on top of the mask. Excitation was performed with a wavelength of 300 nm.

Fluorescence measurements under controlled relative humidities were performed using the relative humidity generator RH-200 from L&C. The humidified argon stream was directed through the measuring cell at 0.5 bar and 500 mL min^{-1}. The selected relative humidities – 20%, 30%, 60% and 90% – were maintained constant for 20 minutes each. Spectra were recorded every 10 seconds.

Powder X-ray diffraction (PXRD) was carried out using a Stoe Stadi P transmission diffractometer operating with Ge(111)-monochromatized $CuK_{\alpha1}$ radiation (λ = 1.54056 Å) and a position sensitive Mythen 1K detector.

Argon physisorption isotherms were measured at 87 K using a Micromeritics 3Flex instrument. The powder samples were outgassed at 120 °C in vacuum immediately prior to the measurement. The BET surface area was determined using the 3Flex Version 5.02 software, enabling the assessment of the relative pressure range for BET according to the Rouquerol plot. The pore width distribution was investigated using NLDFT for cylindrical pore geometry.

Water physisorption isotherms were recorded at 298 K on a vapor 100 °C from 3P instruments. The samples were outgassed at 120 °C in vacuum immediately prior to the measurement.

Scanning electron microscopy (SEM) measurements were performed using a Hitachi Regulus 8230 scanning electron microscope with secondary electrons at 2 kV. The working distance was approximately 10 mm. Energy-dispersive X-ray (EDX) spectra were measured with the integrated EDX-detector Oxford UltiMAX 100 in mapping mode, with a working distance of 10 mm and a measurement time of 5 minutes. Data were quantitatively evaluated using Aztec Version 6.0 software from Oxford Instruments. The powders were fixed on a holder with carbon tape.

The UV-vis measurements were performed using a Cary 4000 from Agilent Technologies equipped with a praying mantis diffuse reflection accessory from Harrick. *In situ* UV-vis measurements were conducted using a reaction chamber placed in the praying mantis diffuse reflection accessory. The relative humidity generator RH-200 from L&C was connected to the gas

port of the reaction chamber, directing the humidified argon stream at 0.5 bar and 500 mL min^{-1} through the device. Relative humidities were adjusted step-by-step, starting with the lowest (20%), maintained for 20 minutes before progressing to 30%, 60% and 90%. Spectra were recorded in the range of 470 nm to 770 nm.

Results and discussion

Impact of the amount of cobalt cations on the fluorescence intensity

To verify that the quenching effect of the europium fluorescence in Eu,Co-MOF-808 is caused by the excitation of d–d transitions of the inserted cobalt cations, we first investigated the correlation between the amount of incorporated cobalt cations and the intensity of the fluorescence of europium cations. To facilitate the incorporation of metal cations, it is beneficial to increase the amount of open coordination sites in MOF-808 by removing non-structural ligands such as modulator molecules from the synthesis prior to post-synthetic modification with metal cations. For instance, this can be efficiently accomplished by solvent exchange with methanol of formic acid-modulated MOF-808 (MOF-808-FA).[26] The amount of formate anions could be reduced from about four to one per IBU in the resulting material, MOF-808 (see Fig. S1a, ESI†), which still retains its crystallinity after the procedure (see Fig. S1b, ESI†).

The post-synthetic modification of MOF-808 was performed by dissolving cobalt(II) chloride hexahydrate in *N,N*-dimethylformamide and soaking the MOF powder in this solution for one hour. To investigate the effect of different amounts of cobalt cations inside the framework on the fluorescence intensity of Eu,Co-MOF-808, the concentration of cobalt chloride hexahydrate was varied from 0.5 eq. to 6 eq. with respect to the Zr_6 cluster of MOF-808. The amount of introduced cobalt cations was determined by EDXS measurements (see Table S1, ESI†) and plotted against the corresponding amount of cobalt cations added to the solution in Fig. 1a. The maximum amount of cobalt cations that can be introduced, approximately 1.5 per IBU, is achieved by adding 3 or more eq of cobalt(II) chloride hexahydrate to the synthesis solution. The addition of 0.5 eq. and 1 eq. of cobalt(II) chloride hexahydrate corresponds to the incorporation of approximately 0.7 eq. and 1.3 cobalt cations per IBU, respectively.

The synthesized Co-MOF-808 powders were subsequently modified with europium(III) nitrate hexahydrate dissolved in acetone for one hour. This resulted in a significant reduction of cobalt cations in the samples (see Fig. 1a). After this procedure, the resulting Eu,Co-MOF-808 powders exhibited residual cobalt content ranging from 0.1 to 0.5 cobalt cations per IBU, depending on the initial amount of cobalt salt added to the synthesis mixture for the respective Co-MOF-808 samples. The introduced amount of europium cations ranged from 1.3 to 1.5 per IBU (see Fig. S2 and see Table S1, ESI†). The structure of MOF-808 remained stable after the modification steps (see Fig. S3, ESI†).

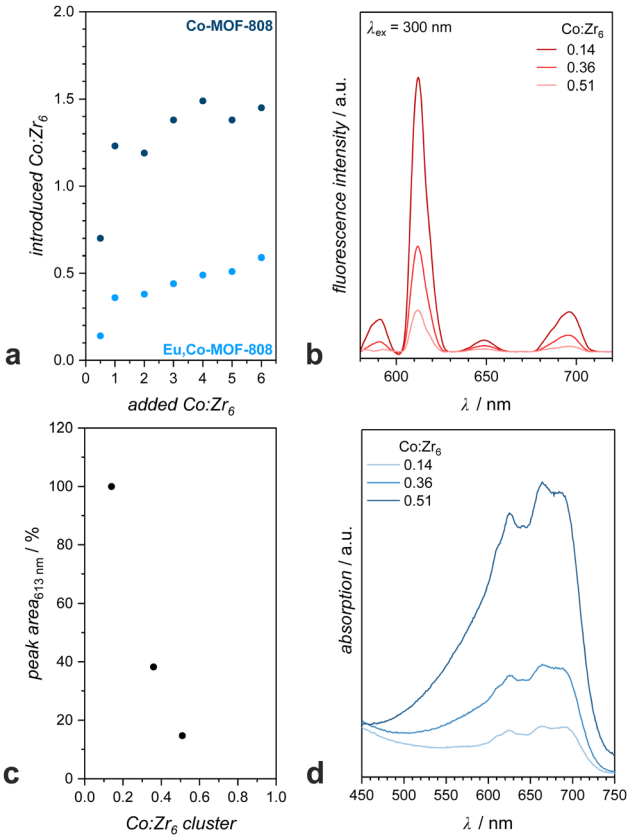

Fig. 1 (a) Amount of incorporated cobalt cations per Zr_6 cluster as a function of the cobalt equivalents added during the synthesis of Co-MOF-808 before (blue) and after (turquoise) insertion of europium cations. (b) Fluorescence spectra of Eu,Co-MOF-808 including different amounts of cobalt cations per Zr_6 cluster. (c) Area of the emission peak of Eu,Co-MOF-808 at 613 nm as a function of the amount of cobalt cations incorporated. (d) UV-vis spectra of selected samples containing different amounts of cobalt cations per Zr_6 cluster.

The influence of incorporated cobalt cations on the fluorescent properties of the materials was investigated by comparing the fluorescence spectra of samples with cobalt contents of 0.14, 0.36 and 0.51 Co:Zr_6 (see Fig. 1b). The intensities were compared by determining the area under the main peak at 613 nm and normalizing all values to that of the material with the highest fluorescence (see Fig. 1c). It was observed that the fluorescence of Eu,Co-MOF-808 diminishes progressively with increasing cobalt content within the framework. Specifically, the emission from the 0.51 Co:Zr_6 sample is more than five times weaker than that of the 0.14 Co:Zr_6 powder, demonstrating that even small variations in the cobalt cation content have a pronounced effect on the fluorescence performance of europium.

We hypothesize that the fluorescence quenching is caused by energy transfer between the incorporated europium and cobalt cations. The radiationless energy transfer from the excited states of the europium cations to the cobalt cations leads to the excitation of d–d transitions. To verify this theory, UV-vis spectra were recorded for the above-mentioned samples (see Fig. 1d). The absorption of the materials is in the range of 500 nm to 750 nm, which completely overlaps with the

wavelength range where the characteristic emission peaks of the europium cations are located. A higher loading of the material with cobalt cations results in a higher absorption intensity in this wavelength range which is accompanied by a reduction in fluorescence intensity (see Fig. 1b).

We previously reported that the initially quenched fluorescence of Eu,Co-MOF-808 can be activated by exposing the sample to a humid atmosphere.[15] Based on this insight into the fluorescence behavior of the system, we performed fluorescence measurements of Eu,Co-MOF-808 in a humid nitrogen stream for five minutes and recorded the UV-vis spectra of the as-synthesized and water-exposed samples (see Fig. S4, ESI†). The fluorescence intensity of the material increases with water exposure, while the absorption intensity of the sample simultaneously decreases in the critical wavelength region. This change coincides with the color change of the powder from blue to light pink.

The increase in fluorescence intensity is due to a less efficient quenching effect of the cobalt cations, as their coordination environment changes from tetrahedral to octahedral upon water exposure.[27] EDXS measurements confirm that the amount of chlorides in the framework remains unchanged after water exposure (see Table S2, ESI†), indicating that the water molecules additionally coordinate to the cobalt cations, altering their coordination geometry. Moreover, the water molecules induce stronger ligand field splitting. As a result, the excitation of the d–d transitions of the generated cobalt complex with higher ligand field splitting energy requires higher energies. Consequently, the energy of the excited states of europium is no longer transferred to the cobalt cations, thus cancelling the quenching effect.

Impact of counter anions coordinating to the inserted cobalt cations

To prove that the type of the cobalt complex at the IBUs is essential for the fluorescence turn-on by water molecules, we also synthesized Co-MOF-808 with cobalt(II) acetate tetrahydrate (Co(OAc)-MOF-808) and cobalt(II) nitrate hexahydrate ($Co(NO_3)$-MOF-808), both structures maintaining high crystallinity after the modification (see Fig. S5, ESI†). Co(OAc)-MOF-808 shows a higher loading of cobalt cations (2 Co:Zr_6) than Co-MOF-808 while $Co(NO_3)$-MOF-808 contains only 0.6 Co:Zr_6. The differing cobalt loadings can be explained by the pH value of the synthesis solutions. A higher pH value allows a more efficient deprotonation of the water molecules and hydroxides attached to the IBUs, enabling more metal cations to coordinate to the generated oxo anions. After introducing europium, the amount of cobalt cations is reduced to 1.5 and 0.3 Co:Zr_6, respectively, while the amount of europium introduced is almost the same (1.1 Eu:Zr_6). The amount of chloride, originating from the chloride-containing synthesis of MOF-808 and coordinating to the IBUs of MOF-808 is about 0.1 Cl:Zr_6, which is significantly lower than for Eu,Co-MOF-808.

The fluorescence change of Co(OAc)-MOF-808 by water exposure (see Fig. S6a, ESI†) is much less pronounced compared to Eu,Co-MOF-808, showing only a slight increase in intensity. The absorption peak of the material is located at 570 nm (see Fig. S7a, ESI†), placing the absorption at higher energies, which significantly reduces the overlap with the emission spectrum of europium. Consequently, the reduction in absorption intensity observed after water exposure has little effect on the fluorescence behavior of the material.

$Co(NO_3)$-MOF-808 shows no absorption peak in the region of the europium emission (see Fig. S7b, ESI†). Accordingly, no fluorescence quenching was observed for this sample. Thus, the material shows the same fluorescence behavior upon exposure to water as Eu-MOF-808:[15] The fluorescence intensity is increasingly quenched by water molecules because the coordination of the water molecule to the first coordination sphere of the europium cations causes energy transfer from europium to the vibrational states of the water molecules (see Fig. S6b, ESI†).

In situ fluorescence and UV-vis measurements under varying relative humidity atmosphere

We have previously reported that the fluorescence intensity of Eu,Co-MOF-808-AA (synthesized using acetic acid as a modulator), which has already been described as a barcode material, can be controlled by the prevailing relative humidity.[15] To confirm that even with this material changes in absorption caused by changes in relative humidity affect the fluorescence of the material, we also present the corresponding *in situ* UV-vis measurements performed in a reaction chamber by applying relative humidities from 10% to 90% for 10 minutes each. The absorption intensity of the material (see Fig. 2a) decreases progressively with higher relative humidities, with the largest changes in the range from 20% to 50%. This suggests that in this relative humidity range, the most pronounced changes in the coordination sphere occur through the coordination of water molecules to cobalt cations. Above a relative humidity of 50%, only small changes in absorbance of about 5% per step can be observed, indicating that further increases of water molecules in the atmosphere have a less significant impact on the coordination sphere of the cobalt cations and that the complex transformation is largely complete.

The fluorescence behavior of the material aligns perfectly with the absorption changes showing the highest increase in fluorescence intensity in the mentioned range of relative humidities (see Fig. 2c). Above 50% RH, the quenching effect is almost abolished because there are almost no cobalt complexes left that are not additionally coordinated by water molecules. This indicates that the d–d transitions are consistent with the emission energy of the europium cations. When comparing the absorption and fluorescence intensities at 614 nm as a function of the applied relative humidities, they correlate perfectly in the opposite direction (see Fig. 2b). This again highlights that the fluorescence behavior of the material is related to the ligand field splitting of the cobalt complex present at the IBUs.

Read-out of Eu,Co-MOF-808-AA by applying different relative humidities

Combining the insight that the amount of incorporated cobalt cations and the prevailing relative humidity have a direct

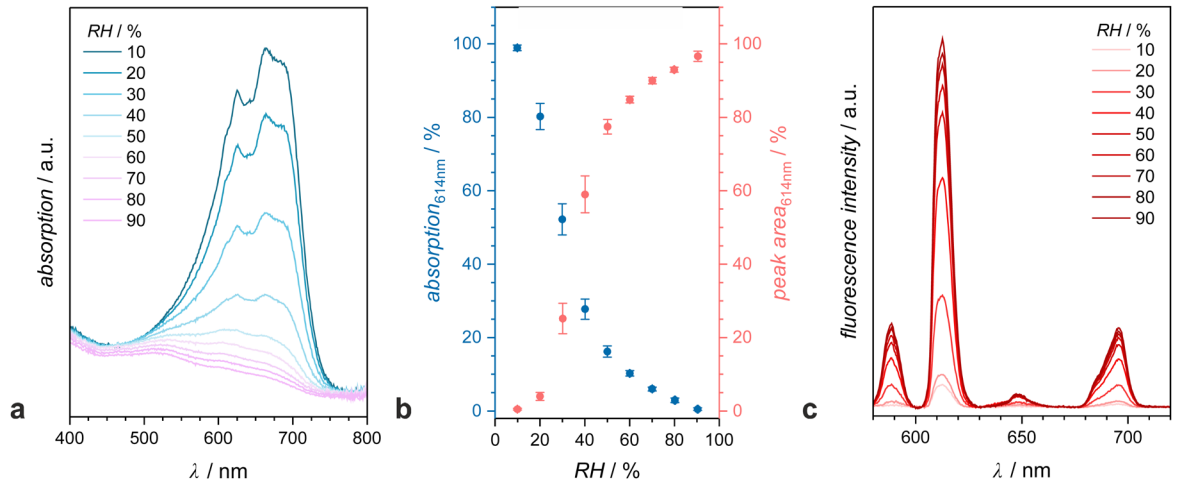

Fig. 2 (a) *In situ* UV-vis measurements, (b) the comparison of absorption intensities and fluorescence peaks areas at 614 nm at different relative humidities and (c) fluorescence measurements of Eu,Co-MOF-808-AA.

influence on the fluorescence intensity of Eu,Co-MOF-808, we want to investigate the potential of the material for the design of a barcode prototype.

For this purpose, we synthesized Eu,Co-MOF-808-AA containing 0.23, 0.39 and 0.45 Co:Zr_6, as described for MOF-808 as the starting material (see Table S3 and Fig. S8, ESI†) since this MOF has already been examined in more detail as barcode material.[15]

The modified materials retain high porosity, confirmed by the BET surface areas, varying from 1370 $m^2\ g^{-1}$ to 1130 $m^2\ g^{-1}$ depending on cobalt content (see Fig. S9a, ESI†). Additionally, the amount of inserted cobalt cations also affects the hydrophilicity of the framework. Compared to the unmodified MOF-808-AA, the materials modified with cobalt and europium cations show higher hydrophilicity. The half adsorption points of the water sorption isotherms range from 0.33 to 0.38, depending on the cobalt content (see Fig. S10a, ESI†). Thus, a higher amount of cobalt results in a more hydrophilic material, which is consistent with the fact that water molecules can coordinate not only to the IBUs, but also to the introduced cobalt cations. Additionally, the area of relative pressure at which water uptake occurs correlates with the area of greatest fluorescence increase, further supporting the relationship between water uptake and the increase in fluorescence.

The materials were exposed to different relative humidities and in each case the change in fluorescence intensity was detected over a period of 20 minutes in 10-second steps. Based on the measurements of Eu,Co-MOF-808-AA (see Fig. 2b), relative humidities of 20%, 30%, 60% and 90% were applied, expecting the most pronounced differences in the fluorescence intensities (see Fig. 3, see Fig. S11, ESI†). Prior to the application of each relative humidity, the samples were heated to 60 °C to return to their initial states.

For this purpose, we synthesized Eu,Co-MOF-808-AA containing 0.23, 0.39 and 0.45 Co:Zr_6, as described for MOF-808 as the starting material (see Table S3 and Fig. S8, ESI†) since this MOF has already been examined in more detail as barcode material.[15]

The modified materials retain high porosity, confirmed by the BET surface areas, varying from 1370 $m^2\ g^{-1}$ to 1130 $m^2\ g^{-1}$ depending on cobalt content (see Fig. S9a, ESI†). Additionally, the amount of inserted cobalt cations also affects the hydrophilicity of the framework. Compared to the unmodified MOF-808-AA, the materials modified with cobalt and europium cations show higher hydrophilicity. The half adsorption points of the water sorption isotherms range from 0.33 to 0.38, depending on the cobalt content (see Fig. S10a, ESI†). Thus, a higher amount of cobalt results in a more hydrophilic material, which is consistent with the fact that water molecules can coordinate not only to the IBUs, but also to the introduced cobalt cations. Additionally, the area of relative pressure at which water uptake occurs correlates with the area of greatest fluorescence increase, further supporting the relationship between water uptake and the increase in fluorescence.

The materials were exposed to different relative humidities and in each case the change in fluorescence intensity was detected over a period of 20 minutes in 10-second steps. Based on the measurements of Eu,Co-MOF-808-AA (see Fig. 2b), relative humidities of 20%, 30%, 60% and 90% were applied, expecting the most pronounced differences in the fluorescence intensities (see Fig. 3, see Fig. S11, ESI†). Prior to the application of each relative humidity, the samples were heated to 60 °C to return to their initial states.

At a relative humidity of 20%, the materials with a cobalt content of 0.39 and 0.45 Co:Zr_6 exhibit a fairly similar fluorescence behavior while the former one showing slightly higher fluorescence intensity, consistent with the quenching effect of the cobalt complexes at the IBUs (Fig. 4a). No remarkable changes in fluorescence compared to the initial state can be detected. The material with a lower cobalt content (0.23 Co:Zr_6) generally shows slightly higher starting fluorescence intensity, which then gradually increases over the initial 10 seconds before stabilizing at a consistent level (see Fig. 3a). The fluorescence tendencies of the materials align with their absorption intensities at 613 nm. While the absorption intensities of the

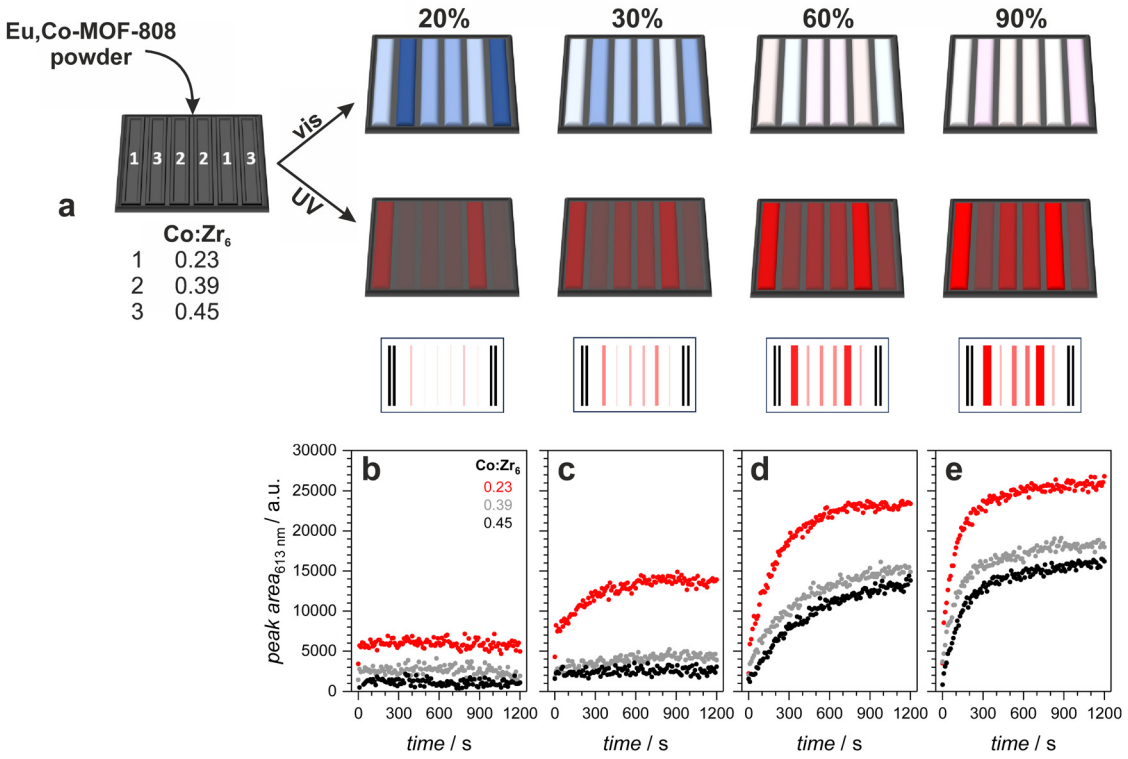

Fig. 3 Design of a barcode prototype based on Eu,Co-MOF-808-AA with varying amounts of cobalt cations. (a) MOF powders with different of cobalt cation concentration are loaded into the marked recesses of the barcode pattern. Exposing the samples to 20, 30, 60 and 90% RH causes a visible color change and fluorescence switching under UV light, dependent on the cobalt content. The intensities of the most intensive fluorescence peak at 613 nm can be converted into widths, thus a barcode can be constructed as read-out answer. (b)–(e) Fluorescence read-out of the samples at the respective relative humidity with an exposure time of 20 minutes.

materials with higher cobalt content are close to each other, that of the material with a cobalt content of 0.23 Co:Zr_6 is distinct lower (see Fig. 4b and Fig. S12, ESI†). Accordingly, for materials with higher cobalt content, a relative humidity of 20% does not allow enough water molecules to penetrate the network and form sufficient cobalt complexes with higher ligand field splitting energy. In contrast, for materials with lower cobalt content, this humidity level is sufficient to increase fluorescence intensity.

When the sample is exposed to a relative humidity of 30%, the fluorescence intensities increase, with the most pronounced increase being observed for the sample with the lowest amount of cobalt cations (see Fig. 3b). Additionally, the deviation of the fluorescence intensities between the sample with 0.23 and those with 0.39 or 0.45 Co:Zr_6 is significantly greater compared to a prevailing relative humidity of 20% (see Fig. 4a). This suggests that the quenching effect decreases as more water molecules coordinate to the cobalt cations. Therefore, lower relative humidities are sufficient to noticeably reduce the quenching effect in materials with fewer cobalt cations. The absorption intensities in the wavelength range, where the europium emission takes place, are already at a low level in the initial state, so slight changes in absorption have a significant impact on fluorescence intensity (see Fig. 4b and Fig. S12, ESI†).

The samples with a higher cobalt content also exhibit a significant increase in fluorescence intensity when exposed to a relative humidity of 60%, with the fastest increase still observed for the material with the lowest cobalt content (see Fig. 3c). Thus, at a relative humidity of 60%, enough water molecules can penetrate the network to largely suppress the quenching effect even for samples with a higher content of cobalt cations. This corresponds to the absorption intensity at 613 nm of the

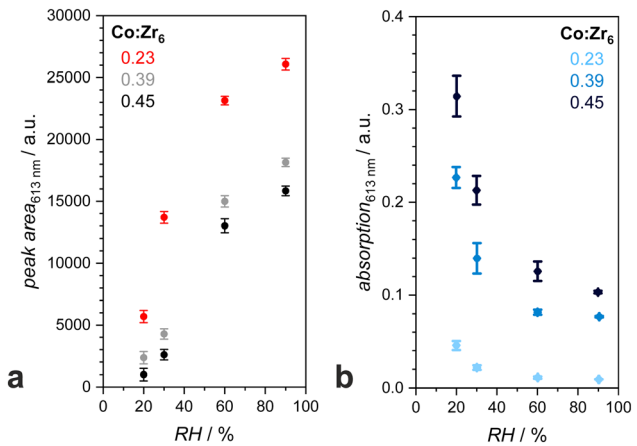

Fig. 4 Average values of (a) fluorescence read-out answers with different cobalt contents at 613 nm calculated from the values detected from 15 min to 20 min after starting the exposure to the respective relative humidities and (b) absorption of Eu,Co-MOF-808-AA.

materials decreasing significantly compared to 20% RH (see Fig. 4b and Fig. S12, ESI†).

Consequently, applying a relative humidity of 90% leads to an even greater and faster increase in fluorescence intensities, as the high proportion of water molecules in the atmosphere allows for the rapid formation of the cobalt complexes with higher ligand field splitting energy (see Fig. 3d). As a result, the amount of cobalt cations present in the framework becomes less relevant to the rate at which maximum fluorescence intensities are reached. It is noticeable that the materials do not show the same fluorescence intensities at this relative humidity, although the framework should be nearly saturated with water molecules, so that all cobalt cations could potentially exhibit an octahedral coordination environment. This can be explained by the fact that the absorption range of the materials is hypsochromically shifted by the formation of the cobalt complex with higher ligand field splitting energy, but still shows slight overlap with the wavelength range in which the emission of europium takes place (see Fig. 4b). Accordingly, materials with a higher cobalt content still exhibit lower fluorescence intensities than those with a lower content at 90% RH (see Fig. 4a).

We have already reported that Eu,Co-MOF-808-AA can be used as a barcode prototype, as its color and fluorescence can be switched in a controlled manner by applying a defined read-out sequence.[15] However, this sequence involves exposure to gaseous ammonia, activation at 120 °C and treatment with gaseous hydrogen chloride, making the barcode read-out not user-friendly due to the involvement of harmful chemicals. As presented here, the fluorescence intensity of Eu,Co-MOF-808-AA can also be simply controlled by the amount of inserted cobalt cations and the predominant relative humidity, offering a new non-hazardous read-out possibility by applying different pre-defined relative humidities to the materials with different cobalt content. As a prototype, the materials containing different amounts of cobalt cations could be arranged in a pattern with vertical grooves in any order (see Fig. 3a). To realize the construction of this barcode prototype, a custom pattern was 3D printed. A matching box with a removable lid was also designed to set the respective relative humidity. This box includes a gas inlet and outlet, allowing direct connection to the humidifier (see Fig. 5a). For the read-out of the constructed barcode, the required relative humidity must be applied and the fluorescence measured after an exposure time of approximately 15 minutes. The fluorescence responses can be converted into a barcode, with the width of the bars correlating with the fluorescence intensities of the materials at the respective positions, as the materials show different emission intensities depending on the amount of incorporated cobalt cations (see Fig. 4a and Fig. S13, ESI†).

To obtain the correct read-out, the fluorescence measurements must be performed at the pre-defined relative humidity. Even small deviations in relative humidity could lead to a barcode showing different bar widths, making it difficult to obtain a correct read-out. However, this variability adds a higher level of security, as the correct read-out can only be obtained under precisely controlled atmospheric conditions. Moreover, the barcode continuously changes its fluorescence and color depending on the predominant relative humidity in the environment, which can also be seen as an advantage in terms of enhancing anti-counterfeit capabilities. Additionally, the materials can be used multiple times without loss of crystallinity and functionality (see Fig. S14a, ESI†). Before each read-out, they should be heated to 60 °C to replace the water molecules already present at the cobalt cations.

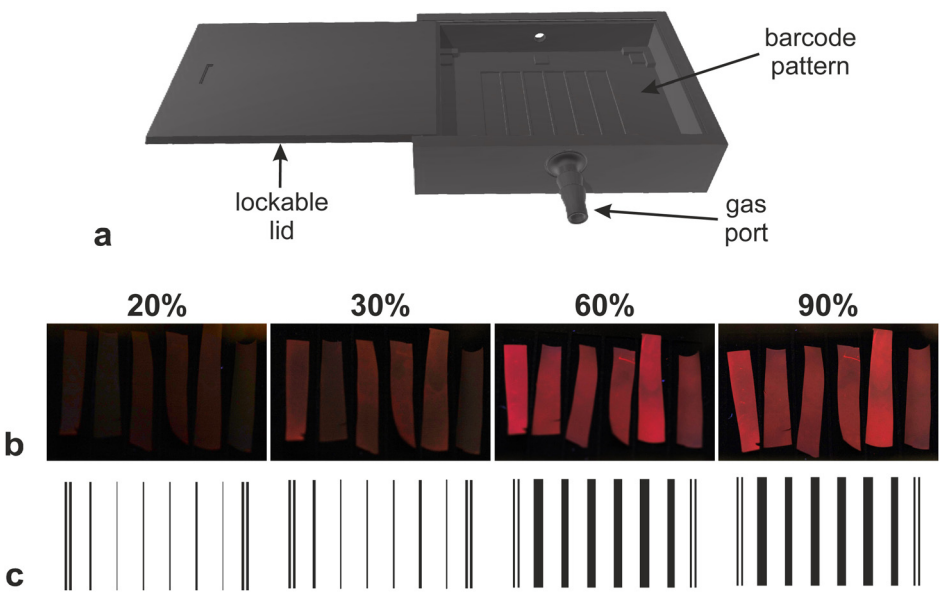

Fig. 5 (a) Illustration of the self-designed 3D printed box with a lockable lid and gas ports including the barcode pattern with six vertical grooves. (b) Pictures of Eu,Co-MOF-808-AA@PVDF stripes placed in the grooves of the barcode pattern in the row 0.23, 0.45, 0.39, 0.39, 0.23, 0.45 Co:Zr_6 at different relative humidities under the UV lamp (254 nm). (c) Calculated peak areas from the measured fluorescence intensities of the main peak at 610 nm (see Fig. S11, ESI†) converted into bar widths, with the smallest width defined as 0.5 pt.

Implementing Eu,Co-MOF-808-AA into polyvinylidene fluoride

We have previously reported that incorporating Co-MOF-808-AA powder into polyvinylidene fluoride (PVDF) and subsequently modifying it with europium cations is an effective way to transform the powder products into a more applicable shape for barcode design, as the framework remains accessible to essential molecules for the read-out.[15] To demonstrate that this concept can also be applied to design a humidity-responsive barcode prototype, mixed-matrix membranes (MMMs) were prepared.

For this purpose, MOF powders with different cobalt amounts were dispersed in acetone while PVDF was simultaneously dissolved in DMF. After mixing these two components and evaporating the solvent under reduced pressure, the resulting MMMs were applied to glass slides using a doctor blade and heated to 70 °C. The Co-MOF-808-AA MMMs were then cut into strips and were modified with europium cations by soaking the pieces in an europium(III) nitrate acetone solution for 10 minutes (see Fig. S15, ESI†). After washing, the final barcode strips were obtained and placed in the designated positions on the barcode pattern, which was housed in the lockable box (see Fig. 5a).

The crystallinity of the materials remained excellent after these procedures (see Fig. S16, ESI†). The relative humidity was adjusted using the humidifier connected to the gas port of the box and kept constant for 20 minutes. The fluorescence of the MMMs changed significantly at higher relative humidities, which was visible under UV light (see Fig. 5b). The measured fluorescence intensities (see Fig. S17, ESI†) could also be converted into bar widths (see Fig. 5c and Table S4, ESI†), enabling the generation of a barcode prototype consisting of six bars, with width that increase with humidity depending on the cobalt content of the materials.

Conclusion

In conclusion, we explained the fluorescence behavior of Eu,Co-MOF-808 by clarifying the interaction between cobalt and europium cations within the framework. The proximity of these cations enables an energy transfer, causing the excitation of d–d transitions of the cobalt cations while simultaneously quenching the fluorescence of europium cations. Thus, the quenching effect is attributed to the d–d transitions of the cobalt cations, with its efficiency depending on the ligands coordinating to the cobalt cations and the coordination geometry of the resulting complex at the IBUs.

The as-synthesized Eu,Co-MOF-808 shows an efficient quenching effect. However, exposure to water reactivates the europium fluorescence. The additional coordination by water molecules changes the coordination geometry of the cobalt complex from tetrahedral to octahedral, shifting the absorption area due to changes in the ligand field splitting.

The targeted suppression of the fluorescence of europium by the presence of cobalt complexes in MOF-808 and its reactivation by introducing ligands that induce energetic changes in the complex, can be exploited for the design of barcode prototypes.

We previously presented a read-out sequence for Eu,Co-MOF-808-AA and its corresponding mixed-matrix membrane as a barcode material, which relied on hazardous chemicals, making it unsuitable for user-friendly applications. Now, we have defined a new read-out procedure which is completely harmless and easy to implement. This material can be used as a dynamic barcode that exhibits defined colorimetric and fluorescent responses to certain relative humidities, depending on the amount of incorporated cobalt cations. This barcode can be easily read by water exposure and reused multiple times by heating the material to 60 °C before read-out.

Additionally, this prototype offers a forgery-proof barcode that dynamically adjusts its read-out response based on the prevailing relative humidity. This ensures a high level of security and accuracy, as the read-out must be performed under controlled conditions, highlighting its reliability and potential for practical applications.

Data availability

The data supporting this article have been included as part of the ESI.†

Conflicts of interest

There are no conflicts to declare.

Acknowledgements

General support and fruitful discussions with Prof. Dr. Peter Behrens are gratefully acknowledged. The authors would like to thank the Hannover School for Nanotechnology (hsn) which is based in the Laboratory for Nano and Quantum Engineering (LNQE) for financial funding and Adrian Hannebauer for performing water sorption measurements.

References

1 (*a*) O. Guillou, C. Daiguebonne, G. Calvez and K. Bernot, *Acc. Chem. Res.*, 2016, **49**, 844–856; (*b*) W. Ren, G. Lin, C. Clarke, J. Zhou and D. Jin, *Adv. Mater.*, 2020, **32**, e1901430.
2 H.-Q. Yin and X.-B. Yin, *Acc. Chem. Res.*, 2020, **53**, 485–495.
3 (*a*) J. Heine and K. Müller-Buschbaum, *Chem. Soc. Rev.*, 2013, **42**, 9232–9242; (*b*) P. Kumar, S. Singh and B. K. Gupta, *Nanoscale*, 2016, **8**, 14297–14340.
4 P. R. Donnarumma, S. Frojmovic, P. Marino, H. A. Bicalho, H. M. Titi and A. J. Howarth, *Chem. Commun.*, 2021, **57**, 6121–6124.
5 Y. Lu and B. Yan, *J. Mater. Chem. C*, 2014, **2**, 7411–7416.
6 (*a*) Y. Gai, Q. Guo, K. Xiong, F. Jiang, C. Li, X. Li, Y. Chen, C. Zhu, Q. Huang, R. Yao and M. Hong, *Cryst. Growth Des.*, 2017, **17**, 940–944; (*b*) P.-F. Zhang, G.-P. Yang, G.-P. Li, F. Yang, W.-N. Liu, J.-Y. Li and Y.-Y. Wang, *Inorg. Chem.*, 2019, **58**, 13969–13978; (*c*) X. Mi, D. Sheng, Y. Yu, Y. Wang, L. Zhao, J. Lu, Y. Li, D. Li, J. Dou, J. Duan and S. Wang, *ACS*

Appl. Mater. Interfaces, 2019, **11**, 7914–7926; (*d*) K. A. White, D. A. Chengelis, K. A. Gogick, J. Stehman, N. L. Rosi and S. Petoud, *J. Am. Chem. Soc.*, 2009, **131**, 18069–18071.

7 (*a*) W. Ding, L. Zhao, X. Yuan, L. Zhang, B. Chen, Q. Ju and Z. Fang, *J. Mater. Chem. C*, 2020, **8**, 3176–3182; (*b*) J. I. Deneff, K. S. Butler, L. E. S. Rohwer, C. J. Pearce, N. R. Valdez, M. A. Rodriguez, T. S. Luk and D. F. Sava Gallis, *Angew. Chem., Int. Ed.*, 2021, **60**, 1203–1211; (*c*) Z.-H. Guo, P.-F. Zhang, L.-L. Ma, Y.-X. Deng, G.-P. Yang and Y.-Y. Wang, *Inorg. Chem.*, 2022, **61**, 6101–6109; (*d*) Y.-M. Wang, X.-T. Tian, H. Zhang, Z.-R. Yang and X.-B. Yin, *ACS Appl. Mater. Interfaces*, 2018, **10**, 22445–22452.

8 P. Zhang, N. Song, S. Liu, Q. Li, Y. Wang and B. Zhou, *J. Mater. Chem. C*, 2021, **9**, 6208–6216.

9 J.-P. Gao, R.-X. Yao, X.-H. Chen, H.-H. Li, C. Zhang, F.-Q. Zhang and X.-M. Zhang, *Dalton Trans.*, 2021, **50**, 1690–1696.

10 C. Li, J. Hai, S. Li, B. Wang and Z. Yang, *Nanoscale*, 2018, **10**, 8667–8676.

11 Z. Gao, B. Xu, T. Zhang, Z. Liu, W. Zhang, X. Sun, Y. Liu, X. Wang, Z. Wang, Y. Yan, F. Hu, X. Meng and Y. S. Zhao, *Angew. Chem., Int. Ed.*, 2020, **59**, 19060–19064.

12 T. Xia, W. Cao, Y. Cui, Y. Yang and G. Qian, *Opto-Electron. Adv.*, 2021, **4**, 200063.

13 J. Othong, J. Boonmak, V. Promarak, F. Kielar and S. Youngme, *ACS Appl. Mater. Interfaces*, 2019, **11**, 44421–44429.

14 Y. Zhang, X. Xu and B. Yan, *J. Mater. Chem. C*, 2022, **10**, 3576–3584.

15 N. Marquardt, F. von der Haar and A. Schaate, *Dalton Trans.*, 2024, **53**, 8608–8618.

16 (*a*) D. Xia, J. Li, W. Li, L. Jiang and G. Li, *J. Lumin.*, 2021, **231**, 117784; (*b*) W. Zhang, J. Xie, Z. Sui, Z. Xu, X. Wang, M. Lei, H. Zhang, Z. Li, Y. Wang, W. Liu, W. Du and S. Wang, *Sci. China: Chem.*, 2021, **64**, 1723–1729; (*c*) Y. Gao, P. Jing, N. Yan, M. Hilbers, H. Zhang, G. Rothenberg and S. Tanase, *Chem. Commun.*, 2017, **53**, 4465–4468.

17 Y. Yu, J.-P. Ma and Y.-B. Dong, *CrystEngComm*, 2012, **14**, 7157.

18 K. Wu, T. Fei and T. Zhang, *Nanomaterials*, 2022, 12.

19 Y. Li, *Polyhedron*, 2020, **179**, 114413.

20 Z. Wang, G. Sun, J. Chen, Y. Xie, H. Jiang and L. Sun, *Chemosensors*, 2022, **10**, 66.

21 D. Wang, Q. Tan, J. Liu and Z. Liu, *Dalton Trans.*, 2016, **45**, 18450–18454.

22 (*a*) L. Qin, S. Zhou, Y. Zhou and L. Han, *J. Solid State Chem.*, 2019, **277**, 658–664; (*b*) F. Drache, V. Bon, I. Senkovska, M. Adam, A. Eychmüller and S. Kaskel, *Eur. J. Inorg. Chem.*, 2016, 4483–4489.

23 M.-H. Zeng, Y.-X. Tan, Y.-P. He, Z. Yin, Q. Chen and M. Kurmoo, *Inorg. Chem.*, 2013, **52**, 2353–2360.

24 (*a*) Philippa A. Brayshaw, Jean-Claude G. Buenzli, Pascal Froidevaux, Jack M. Harrowfield, Yang Kim and Alexander N. Sobolev, *Inorg. Chem.*, 1995, **34**, 2068–2076; (*b*) T. S. Atabaev, O. S. Jin, J. H. Lee, D.-W. Han, H. H. T. Vu, Y.-H. Hwang and H.-K. Kim, *RSC Adv.*, 2012, **2**, 9495; (*c*) M. C. Stoian, I. Mihalache, M. Matache and A. Radoi, *Dyes Pigm.*, 2021, **187**, 109144; (*d*) S. Shuvaev, M. Starck and D. Parker, *Chem. – Eur. J.*, 2017, **23**, 9974–9989.

25 X. Liu, K. O. Kirlikovali, Z. Chen, K. Ma, K. B. Idrees, R. Cao, X. Zhang, T. Islamoglu, Y. Liu and O. K. Farha, *Chem. Mater.*, 2021, **33**, 1444–1454.

26 C. Jia, F. G. Cirujano, B. Bueken, B. Claes, D. Jonckheere, K. M. van Geem and D. de Vos, *ChemSusChem*, 2019, **12**, 1256–1266.

27 (*a*) M. Uchikoshi, *J. Solution Chem.*, 2018, **47**, 2021–2038; (*b*) J. A. Botas, G. Calleja, M. Sánchez-Sánchez and M. G. Orcajo, *Langmuir*, 2010, **26**, 5300–5303.

